Anisotropic, Transparent Films with Aligned Cellulose Nanofibers

*Mingwei Zhu, Yilin Wang, Shuze Zhu, Lisha Xu, Chao Jia, Jiaqi Dai, Jianwei Song, Yonggang Yao, Yanbin Wang, Yongfeng Li, Doug Henderson, Wei Luo, Heng Li, Marilyn L. Minus, Teng Li, and Liangbing Hu**

Transparent films or substrates are ubiquitously used in photonics and optoelectronics, with glass and plastics as traditional choice of materials. Transparent films made of cellulose nanofibers are reported recently. However, all these films are isotropic in nature. This work, for the first time, reports a remarkably facile and effective approach to fabricating anisotropic transparent films directly from wood. The resulting films exhibit an array of exceptional optical and mechanical properties. The well-aligned cellulose nanofibers in natural wood are maintained during delignification, leading to an anisotropic film with high transparency (≈90% transmittance) and huge intensity ratio of transmitted light up to 350%. The anisotropic film with well-aligned cellulose nanofibers has a mechanical tensile strength of up to 350 MPa, nearly three times of that of a film with randomly distributed cellulose nanofibers. Atomistic mechanics modeling further reveals the dependence of the film mechanical properties on the alignment of cellulose nanofibers through the film thickness direction. This study also demonstrates guided liquid transport in a mesoporous, anisotropic wood film and its possible application in enabling new nanoelectronic devices. These unique and highly desirable properties of the anisotropic transparent film can potentially open up a range of green electronics and nanofluidics.

Many optoelectronic and microfluidic devices are built on transparent substrates, for which glass and plastics are typically used. Recently, Corning developed transparent and flexible slim glasses, which can possibly enable roll-to-roll processing.[1] Transparent biodegradable films made of cellulose nanofibers and chitin have also been developed.[2–10] All these transparent substrates are isotropic in nature, i.e., the optical and mechanical properties are independent of the orientation of the planar substrates.[11] For example, when a liquid drop is applied on the surface of plastics or glass, it diffuses or spreads evenly without any preferred directions. Transparent films with anisotropic properties, however, can enable new micro/nanofluidic and optoelectronic device concepts. For example, if directional liquid transport is possible without building external channels (as used by Whitesides and co-workers in their paper fluidic devices[12–14]), new microfluidic configurations are possible to significantly simplify device fabrication and manufacturing. Anisotropic transparent substrates can also have unique effects on guided light distribution for display and lighting applications.[15] Enthusiasm for these new device concepts aside, fabrication of transparent substrates with anisotropic nanostructures and properties remains as a challenge.

Trees transport water and minerals efficiently through their anisotropic wood structures. Wood is mainly composed of lumina cell fibers with typically 3–5 mm in length and 25–50 μm in diameter. For almost all types of trees, the wood cell fibers are roughly aligned in the tree growth direction.[16] Each wood cell fiber contains multiple microfibers and each microfiber can further be broken down into nanosized fibers, i.e., cellulose nanofibers (CNFs).[4,6,7,17–20] Besides their abundance and biodegradability, CNFs have a high aspect ratio and rich surface chemistry for facile functionalization, making them a promising building block for a range of functional materials, such as transparent paper,[7–11,21,22] energy storage devices,[23] lightweight aerogels,[24] and strong and tough composites.[4,25,26] The fabrication of these functional materials often involves two steps. First, CNFs are extracted from wood through chemical,[27] mechanical,[28] or biological methods.[29] However, these methods to extract CNFs consume much energy and time. Second, the extracted CNFs in solution are then dried by removing water to form functional materials (e.g., transparent paper), a process that also requires much energy and time. The

Prof. M. Zhu, Dr. Y. Wang, L. Xu, C. Jia, J. Dai, J. Song, Y. Yao, Y. Wang, Prof. Y. Li, D. Henderson, Dr. W. Luo, Prof. L. Hu
Department of Materials Science and Engineering
University of Maryland
College Park, MD 20742, USA
E-mail: binghu@umd.edu
Dr. S. Zhu, Prof. T. Li
Department of Mechanical Engineering
University of Maryland
College Park, MD 20742, USA
H. Li, Prof. M. L. Minus
Department of Mechanical and Industrial Engineering
Northeastern University
Boston, MA 02115, USA

DOI: 10.1002/adma.201606284

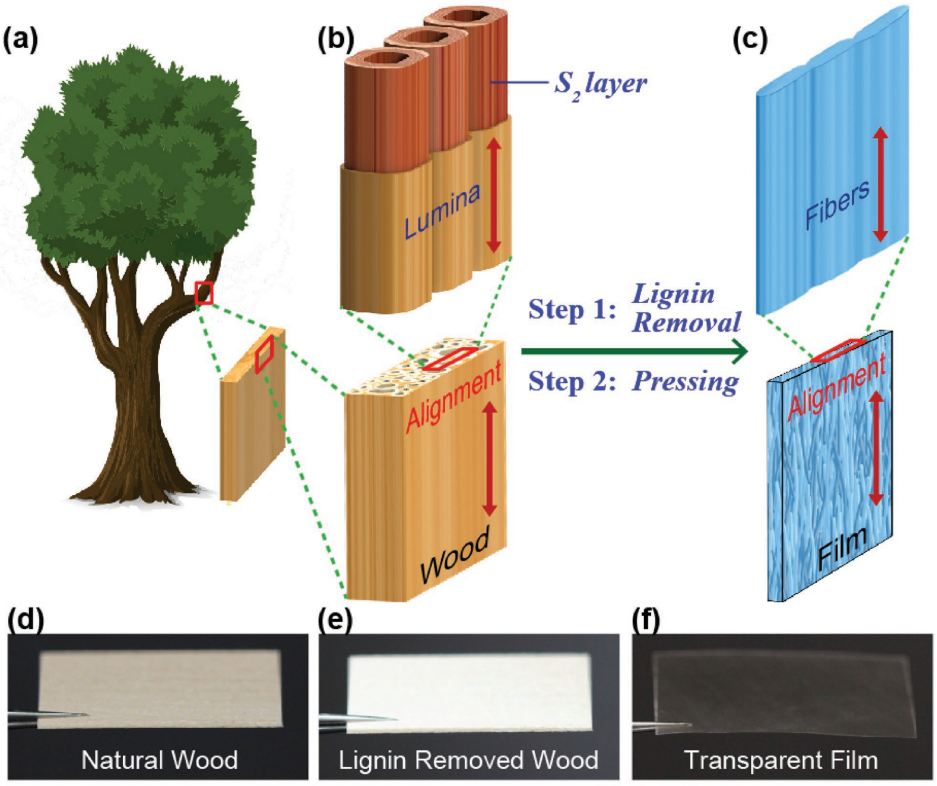

Figure 1. Schematic of direct transformation of an anisotropic wood slice into an anisotropic transparent film by lignin removal and mechanical pressing. a) Wood microstructures. Wood lumina are aligned and fibers in S_2 layer are also aligned. b) The two-step fabrication process. Step 1: lignin removal, which leads to the change of wood color from yellow to white while maintaining the cellulose framework in natural wood. Step 2: mechanical pressing, which leads to about a five time thickness reduction. c) The lumina are fully closed after mechanical pressing. During Step 1 and Step 2, both the microscale alignment for lumen and the nanoscale alignment for CNFs in natural wood are well preserved in the resulting transparent film. d–f) Photos of the color changes from (d) yellow natural wood to (e) white wood and finally to a (f) transparent film.

resulting functional materials consist of randomly distributed CNFs and thus are isotropic in nature. In short, the existing CNF-based functional materials are fabricated via a complex and expensive approach and the highly aligned CNF structure in wood is lost during processing.

Here we demonstrate an extremely straightforward method to fabricate anisotropic films with highly aligned CNFs by delignification and mechanical pressing of natural wood. Amazingly, the CNFs can be well maintained in their original direction in natural wood, leading to a thin, transparent film with outstanding anisotropic properties. Compared with transparent nanopaper with randomly distributed CNFs,[4,5,7,11,25,30] the transparent, anisotropic film has anisotropic mesostructures that can guide liquid transport, allow for anisotropic effects in light transmittance, and enhance mechanical properties. In particular, the fabrication process includes two steps: first wood delignification in NaClO (in water) solution and then mechanical pressing, which is much simpler and consumes less energy and time compared with that of previously developed transparent paper.[7–11,21,22]

A natural wood typically consists of lignin, hemicellulose, and cellulose, which are organized into a highly hierarchical structure (**Figure 1**a,b). In wood cell walls, CNFs with a diameter of less than 10 nm self-organize along different directions. Most fibers grow in an aligned way in various cell wall layers (see Figure S1, Supporting Information). However, the second layer (S_2) in lumen makes up the largest portion of the wall thickness and affects the physical properties of wood the most. The nanofibers are well aligned in the S_2 layer with a direction in a certain angle away with the wood growth direction. Microfibril angle (MFA), defined as the angle between the direction of the helical windings of cellulose microfibrils in S_2 layer and the long axis of cell wall, is usually used to describe the aligned cellulose microfibrils in wood.[16,31] We cut the wood along its growth direction, therefore the macroscopic wood channels are in the plane of the wood blocks (Figure 1b). We carefully remove the yellowish lignin in wood by in situ NaClO treatment without destroying the macroscopic structures with well-aligned channels (Figures S2–S4, Supporting Information). After delignification, the wood becomes white in color and mainly consists of CNFs. Most CNFs align along a direction with an angle of MFA with respect to the tree growth direction. After lignin removal, mechanical pressing was applied to densify the white wood film with about a five time reduction in thickness, which leads to a highly transparent film with highly aligned CNFs (Figure 1c–f; Figure S5, Supporting Information). Note that raw materials of wood have similar anisotropic microstructures despite their properties of species, age, inner or outer parts, lower or higher parts, etc. This two-step fabrication process can be generally applied to fabricate anisotropic films

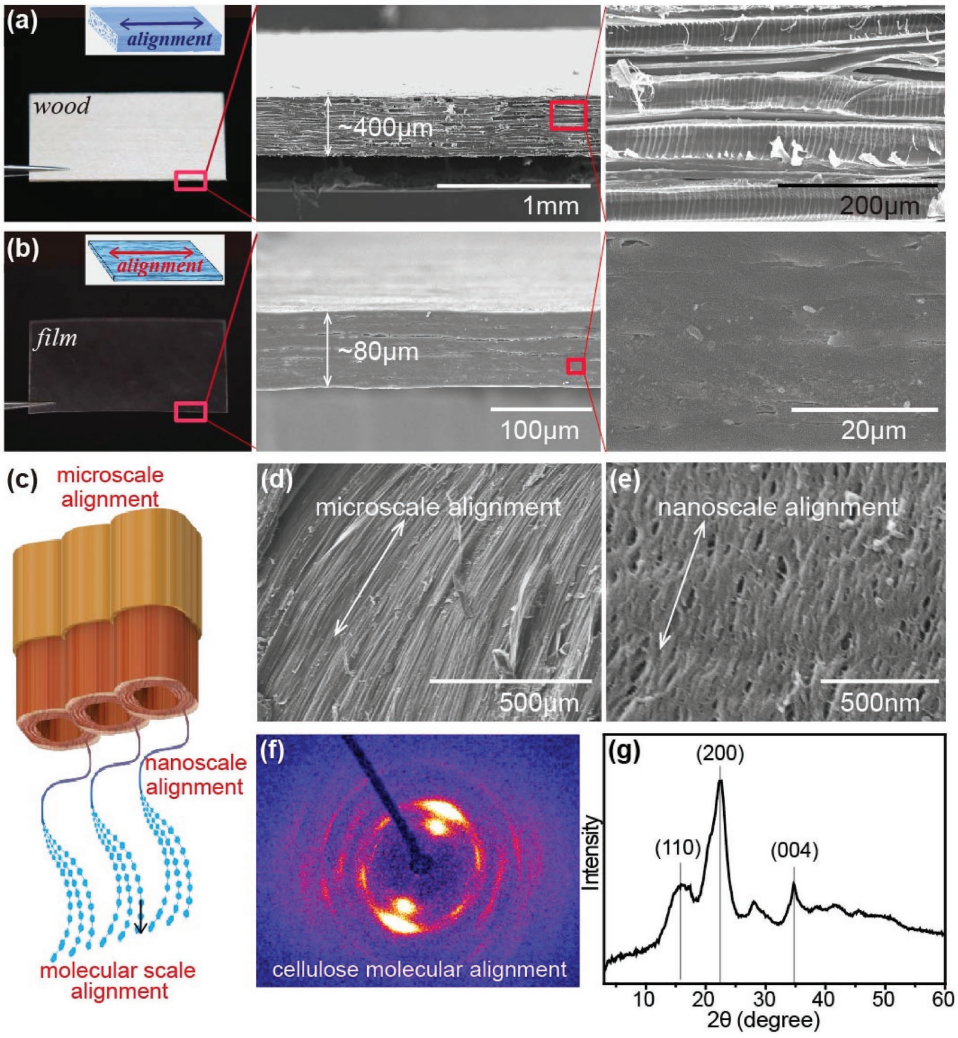

Figure 2. Characterization of microstructures of delignified wood and the resulting anisotropic transparent film. a) Photo and SEM images of delignified white wood before pressing. Lumina alignment is clearly observed in the white wood. b) Picture and SEM images of transparent film pressed from the white wood. It is dense and the anisotropic property is well preserved. c) Schematic of the wood cell microstructures. The second layer (S_2) makes up the vast majority of the cell wall, the nanofibers are aligned with a microfibril angle (MFA) deviated from lumina axis. d) SEM image of the inner part of the transparent film, showing the aligned microfibers. e) SEM image of the transparent film, showing the aligned nanofibers. f) XRD pattern of the transparent film showing the anisotropic alignments of cellulose chains. g) XRD of the transparent film, showing its main component of cellulose.

with wood-specific processing conditions. We have extended our study from basswood (a typical hardwood) to pine wood (a typical softwood) for further demonstrations (Figure S6, Supporting Information).

The CNF alignment in the transparent film finds its origin in the alignment of the fibers in wood cell walls. As shown in **Figure 2**a, the microscaled lumina in wood are highly aligned along the wood growth direction. The cutting across the lumina shows their length can reach about several millimeters with aligned channels. After removing the lignin and pressing the wood, the lumina channels disappear and the wood becomes a dense film with a low surface roughness (Figure 2b; Figure S7, Supporting Information). However, the alignment of fibers is well preserved. As shown in Figure 2c, wood has a complex and delicate hierarchical structure. The unit cell in wood is well aligned and the cell wall is composed of numerous well-aligned micro- and nanofibers. The axis of the cell is along the wood growth direction. However, most of micro- and nanofibers are tilted along the lumina axis direction with a certain angle deviation of MFA.[16] Most of the micro- and nanofibers in the cell walls are highly aligned. During pressing, these aligned micro- and nanofibers are precisely transferred to the transparent film.

By tearing to expose the inner part of the film (Figure 2d), the alignment of microfibers can be clearly observed. The alignment of nanofibers is also well preserved in the film (Figure 2e; Figure S8, Supporting Information). Because the aligned S_2 layer makes up the vast majority of the cell wall, the CNFs in the resulting film exhibit strong alignment. In accordance, most cellulose molecule chains show preferred alignment within the film, which is supported by the X-ray diffraction (XRD) analysis and shown in the wide-angle pattern (Figure 2f; Figure S9, Supporting Information). It shows highly anisotropic distribution

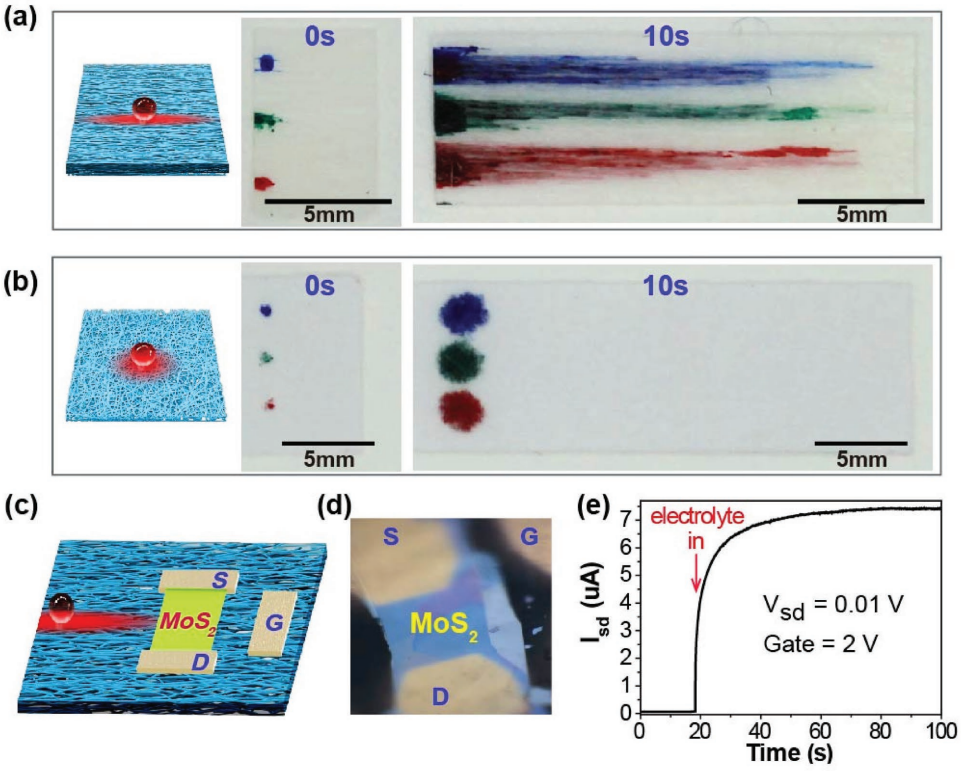

Figure 3. Anisotropic mass transport and applications in microfluidic type of device—liquid electrolyte-gated MoS_2 transistor on an anisotropic transparent film. a) The dispersion of colored water on the surface of the anisotropic film, showing the directional flow of water. b) The dispersion of color water on the surface of an isotropic paper, showing the random diffusion of water. c) Schematic working principle of the device, where anisotropic film guides the electrolyte flow in an anisotropic way to trigger the circuit. d) The optical microscope image of the device fabricated on the surface of the anisotropic film. e) Experimental result of the current between source and drain with the gate triggered by electrolyte.

of the scattering intensity. The film represents the typical cellulose structure in natural wood indicated by XRD measurement (Figure 2g). Peaks around $2\theta = 16.5°$, 22.5°, and 34.6° correspond to cellulose crystals with characteristic assignments of (110), (200), and (004) planes, respectively.[32] The delignination and pressing fabrication processes do not change the cellulose molecules and their arrangements. Compared with recent development on cellulose nanofibril alignment by combining hydrodynamic alignment with a dispersion–gel transitions,[33] our method can be more scalable.

The resulting anisotropic film shows anisotropic properties that stem from the highly aligned microstructures. For example, the anisotropic film can guide the liquid, which results in an anisotropic mass transport. As shown in **Figure 3**a, when the liquid is dipped on the surface of the anisotropic film, the droplet spreads along the direction of fiber alignment, suggesting that the liquid is guided by the fibers along the alignment direction, while it is blocked along the perpendicular direction. By contrast, for the isotropic film made of randomly packed hydrophilic cellulose fibers shown in Figure 3b, the liquid droplet spreads in all directions. Functional materials can be transported by the liquid to a targeted destination for a range of applications such as targeted drug delivery and microfluidic paper diagnostics.[12,34,35] To demonstrate this intriguing feature, we designed an anisotropic mass-transport-triggered circuit based on MoS_2 (Figure 3c). The MoS_2 thin flake is obtained by mechanical exfoliation on the anisotropic film and the electrical contacts are defined with a shadow mask (Figure 3d). The working principle is that, in an electrolyte-gated MoS_2 device, an electrical double layer is formed at the electrolyte/MoS_2 interface to tune the carrier density in the MoS_2 flake, therefore tuning the conductivity of the MoS_2 device. As shown in a schematic in Figure 3c, the electrolyte (polyethylene oxide (PEO)/$LiClO_4$) directionally spreads on the surface of the anisotropic paper and gradually covers the MoS_2 device. The source–drain current increases about two orders of magnitude after adding the electrolyte, as shown in Figure 3e, indicating the successful turn-on of the MoS_2 transistor. The resulting circuit realizes the goal of triggering the device by anisotropic mass transport on the surface of an anisotropic film.

The transparent film with aligned CNFs directly inherited from natural wood shows dramatic anisotropic optical properties. As shown in **Figure 4**a, when light passes through the anisotropic film, the intensity of light distribution is in sharp contrast along the two directions with huge intensity ratio up to 350% (Figure S10, Supporting Information). The light is scattered more strongly in the direction perpendicular to the fiber alignment. Such anisotropic light scattering exhibits unique imaging effects. We designed a pattern with grid lines to show the imaging effects of the transparent anisotropic film (Figure 4b,c). When the anisotropic film is placed 5 mm above the grid lines, only parallel lines can be observed and the

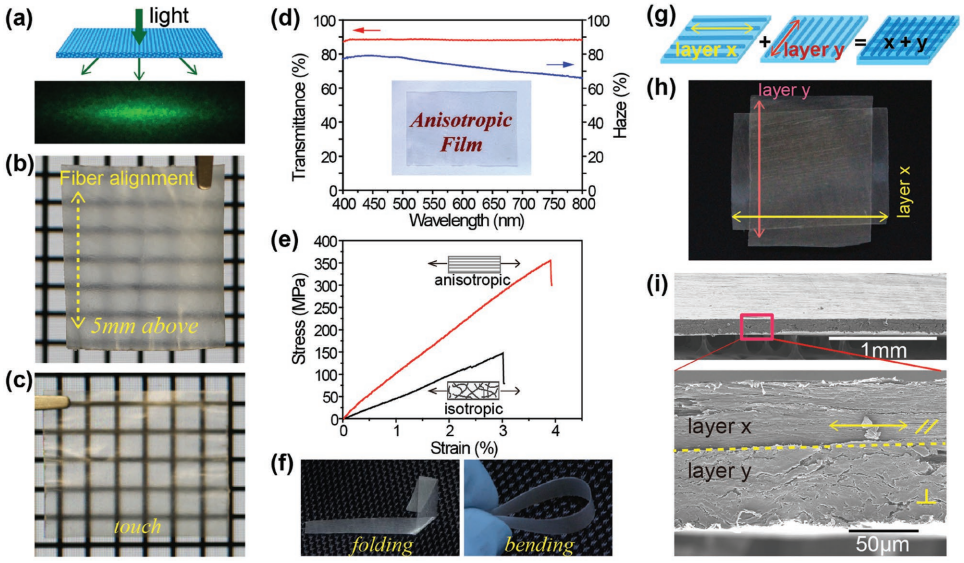

Figure 4. The anisotropic optical and mechanical properties of the transparent film. a) A photo image of the scattered light spot, showing light is scattered by the anisotropic film in an anisotropic manner. b) The anisotropic film is placed 5 mm above the grids. Parallel lines are more visible than vertical lines due to the anisotropic light scattering. c) The anisotropic film is placed directly on the grids. By contrast, both the parallel and vertical lines are clearly seen. d) Diffused transmittance and transmittance haze of the anisotropic film with a thickness of about 50 μm. The inset shows that the writing underneath the anisotropic film is clearly seen. e) The stress–strain curves of the transparent anisotropic film and an isotropic nanopaper. f) Photo images of (a) folding and (b) bending of the anisotropic, transparent film. g) Schematic of a multilayered transparent film with perpendicular fiber alignments. h) The fabricated double-layer anisotropic transparent film. i) SEM image of the double-layer anisotropic transparent film. The fiber alignment direction of top and bottom layers is perpendicular to each other.

vertical lines are diminished. However, all the grid lines can be clearly seen when the anisotropic film contacts the pattern. Such a selectivity may find applications in certain conditions. Also, the film exhibits polarization effects (Figure S11, Supporting Information) originating from the cellulose fiber alignment. The anisotropic film is highly transparent (Figure 4d) and uniform in terms of transparency (Figure S12, Supporting Information). The total transmittance is nearly 90% across the measured wavelengths from 400 to 800 nm. The writing letters beneath the film can be clearly seen (Figure 4d, inset). Such high transparency is attributed to the changes in both components and microstructures during the transition from wood to film. First, absorption is eliminated by removing the colored lignin component. Second, the light scattering is successfully suppressed by pressing porous wood (Figure 2a) to dense film (Figure 2b). The transparent film also exhibits high haze in the range of measured wavelengths. Such anisotropic optical properties are in accordance with the anisotropic microstructure of the transparent film. The CNFs are densely packed and the nanospaces between them cannot efficiently scatter light, leading to the high optical transmittance. Also, the anisotropic refractive index in film makes light be scattered in an anisotropic way, which is also in accordance with the anisotropic microstructures of the transparent film. Such an anisotropic optical property may have potential applications, thin-film optoelectronics,[36] for example.

The transparent film also exhibits superb mechanical properties (Figure 4e). The transparent film with aligned CNFs has a high fracture strength (≈350 MPa), nearly three times of that of a nanopaper with randomly distributed CNFs (made from the same kind of wood, shown as a control in our experiments). Its fracture strength is even about 25% higher than nanopaper (≈280 MPa), which is made of small CNFs through a time- and energy-consuming bottom up approach.[37] Note that the fracture strength in the direction perpendicular to the CNF alignment is about 23.2 MPa (Figure S13, Supporting Information). The aligned film also has better ductility than that of the random film. As a result, the toughness of the anisotropic film (7.38 MJ m^{-3}) is about 3.3 times of that of the random film (2.21 MJ m^{-3}). The anisotropic film fabricated by our top-down approach is also foldable and flexible (Figure 4f). The anisotropic film as a building block by directly pressing delignified wood also allows us to fabricate stacked layered structures with different orientations among the layers. A stacked film by perpendicularly stacking the aligned films is shown in Figure 4g. By stacking a film with fiber alignment in x direction followed by y direction, an x–y directional anisotropic film with double layers is fabricated (Figure 4h). The two layers can be seamlessly integrated during the wet-pressing step. The anisotropic structure for each layer (x and y layer) can be clearly observed by scanning electron microscope (SEM) (Figure 4i; Figure S14, Supporting Information).

The structural anisotropy in the film can be tailored by tuning the cutting direction in wood raw materials. As shown in **Figure 5**a, the wood growth direction (also the lumina direction) is fixed and the cutting direction can be varied. Here θ is defined as the angle of the cutting direction and the wood growth direction. Regardless of the cutting direction, when the wood slice is pressed to a much thinner film, the alignment of fibers will be preserved. Different θ in natural wood corresponds to different fiber alignment γ in film, where γ is defined as the angle of the fiber direction and the film surface

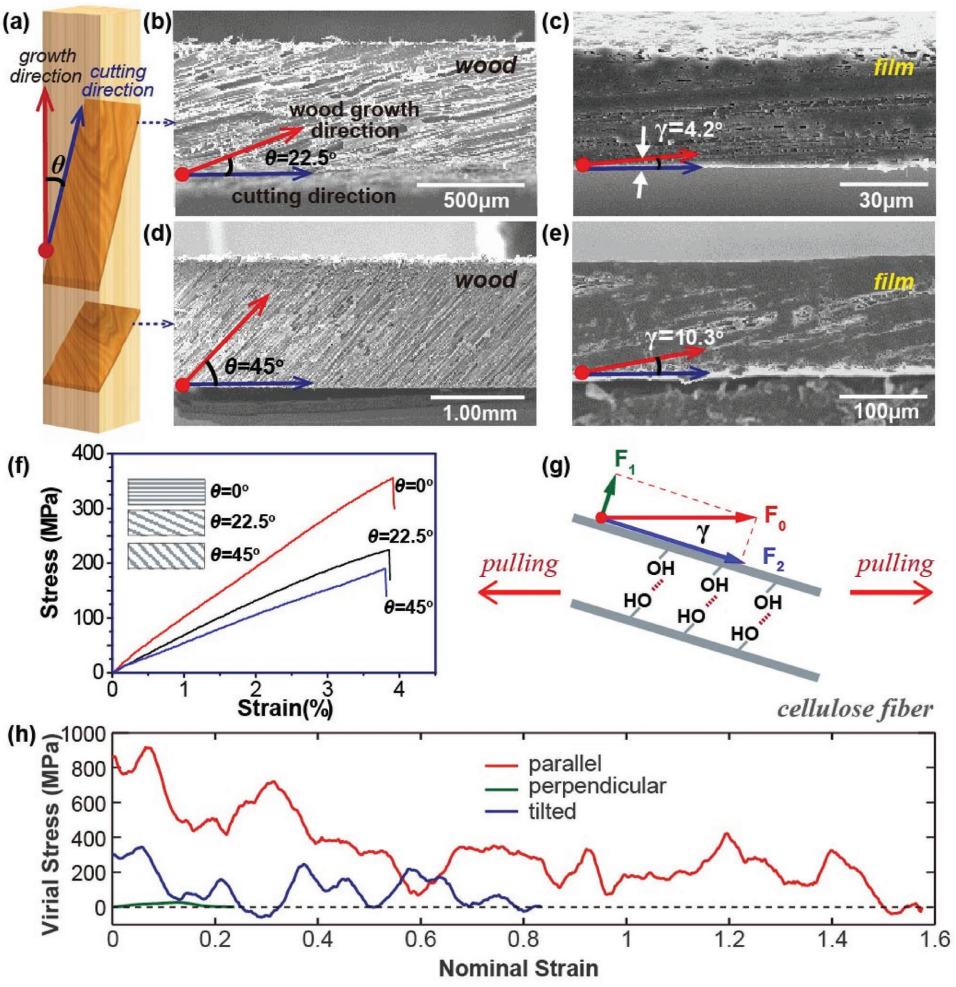

Figure 5. Tunable anisotropic structures by simple changing the cutting direction before the two-step process (i.e., delignification and pressing). a) Different wood slices can be obtained by selecting different cutting directions, which result in different transparent films with different fiber alignments. b,c) 22.5° cutting wood slice and the corresponding transparent film, respectively. d,e) 45° cutting wood slice and the corresponding transparent film, respectively. f) Experimental stress–strain curves of the anisotropic films with different wood cutting angles of 0°, 22.5°, and 45°. g) Schematic illustration of the forces between adjacent fibers in the anisotropic film with alignment angle γ when a force is applied. h) Averaged virial stress per atom calculated from MD simulation as a function of the strain applied to the simulation box. Red lines correspond to the case that the stretching is parallel to the alignment direction. Green and blue lines indicate that the stretching is perpendicular or having a tilted angle to the alignment direction.

direction. The relationship between θ and γ is described as following

$$\tan(\theta) = A \tan(\gamma) \quad (1)$$

where A is the pressing coefficient, defined as the ratio of the wood thickness to the film thickness, and is experimentally found to be about 5 for all the pressed films. Obviously, a large θ in wood leads to a large γ in the film. Here θ of 22.5° and 45° are selected as typical cutting angles to demonstrate the tenability of film anisotropy. As shown in Figure 5b–e, the resulted γ in the anisotropic film are 4.2° and 10.3°, respectively, which are well in accordance with Equation (1). Hence, the fiber alignment in film can be readily tuned by simply adjusting the cutting angle θ (Figures S15–S17, Supporting Information), and the angle γ will be altered in accordance. This provides a facile method to accurately design and fabricate films with a desired anisotropic property. The films with a varying angle γ have their unique anisotropic microstructures, which may lead to different anisotropic properties. For example, the mechanical property varies with different fiber alignment γ in films. As shown in Figure 5f, the maximum stress increases greatly with decreasing fiber alignment γ. Figure 5g illustrates the stress state for the fibers in the film with fiber alignment γ. When the pulling force is applied along the film, the force will be transferred to the fibers. The applied force F_0 can be decomposed into two components: force F_1 perpendicular to the fiber direction and force F_2 parallel to the fiber direction. They have different effects on the fibers. The force F_1 perpendicular to the fiber direction tends to separate adjacent fibers and the force F_2 parallel to the fiber direction pulling the fiber. At the molecular scale, the forces to balance F_1 and F_2 are the hydrogen bonds formed between the adjacent fibers and the covalent bonds within cellulose fibers, respectively. As is shown, the covalent

bond is much stronger than the hydrogen bond. For $\gamma = 45°$, F_1 and F_2 are equal and the film tends to be torn and broken. With the decrease of γ, at the same force F_0, the force F_1 decreases while the force F_2 increases correspondingly. Hence, more loadings are applied onto the fibers. For $\gamma = 0°$, all the loadings are applied onto the fibers and no force is applied between the adjacent fibers.

To qualitatively shed light on the underlying deformation mechanism, we performed molecular dynamics simulations on a scaled-down model,[38,39] which contains well-aligned cellulose chains in a periodic simulation box (see Figures S18 and S19 of the Supporting Information for additional details). The averaged virial stress, which is commonly used to relate to the macroscopic (continuum) stress in molecular dynamics computations,[40,41] is computed for each atom in the system, including stretching directions parallel, perpendicular, or tilted with respect to the fiber alignment direction. As shown in Figure 5h, the simulated results show drastic differences in both strength and toughness (area underneath the curve). The maximum stress in the parallel case is 3.65 times and 34 times of that of the tilted case and perpendicular case, respectively. The toughness in the parallel case is 6 times and 164.6 times of that of the tilted case and perpendicular case, respectively. Such a significant difference is caused by the anisotropic film microstructures, which is confirmed by a further investigation on the deformation trajectory (see Figures S18 and S19 of the Supporting Information for additional data). For the parallel case, we could observe a maximized number of interfaces at which each individual cellulose chain could slide over each other. The sliding is accommodated by breaking the hydrogen bonds. The more of these interfaces there are, the larger the mechanical load the structure as a whole could transfer, leading to an enhanced strength. Accordingly, more energy is dissipated toward fracture and leads to greatly improved toughness. On the contrary, the interchain sliding for the perpendicular case is significantly reduced. A through-crack forms quickly once the two chains are separated beyond the effective range of the hydrogen bonds. As a result, the amount of dissipated energy reduces significantly and so is the load-transferring capacity, leading to minimum strength and toughness. The tilted case is an intermediate scenario between these two limiting cases.

In conclusion, for the first time, we have fabricated anisotropic transparent films with aligned cellulose nanofibers by an extremely simple but effective method. The natural alignment of CNFs in wood is well preserved during the delignification and mechanical pressing processes, which is confirmed using XRD analysis. The alignment of CNFs in the transparent films leads to highly anisotropic transmittance and guided liquid transport. The alignment of CNFs also leads to a dramatic increase in mechanical strength and toughness of the resulting anisotropic film, compared with its counterpart without alignment. Complementary mechanical modeling reveals the molecular scale strengthening and toughening mechanisms in the resulting anisotropic films. We demonstrated a unique electrolyte-gated MoS_2 transistor on the highly transparent, anisotropic film that can be turned on by guiding liquid along the alignment direction. The simple, scalable, energy and time efficient method for fabricating the anisotropic, transparent, and biodegradable films directly from natural wood will unlock a range of new green electronics and fluidic devices.

Experimental Section

Materials and Chemicals: Basswood and pine wood pieces with a size of 2 in. × 2 in. were used in this study. The sodium hypochlorite solution used for removing lignin contents from wood was from Sigma-Aldrich (reagent grade, available chlorine 10%–15%). The PEO (M_w = 100 000) and $LiClO_4$ used in this study were from Sigma-Aldrich.

Transparent Film Fabrication: The wood slices were immersed in the sodium hypochlorite solution for 3–5 h (wood: NaClO = 1:40 wt). After the wood slices turned to white, they were washed by the solution of water and ethanol (1:1 wt) for three times. The lignin removed wood slices were then covered with microporous filtering film and filter paper. Finally, they were pressed at different pressure for about 1–3 h to obtain anisotropic films.

Electrolyte-Gated MoS_2 Transistor: The thin MoS_2 flakes were exfoliated from a bulk MoS_2 crystal by a scotch tape method and then transferred to the transparent anisotropic wood film. Contact electrodes were made of 50 nm Au by a shadow mask method, to avoid contaminants introduced by standard lithography processes. The electrolyte consisting of $LiClO_4$ and PEO was prepared in the weight ratio 0.12:1. The electrolyte was mixed with methanol and then stirred overnight at room temperature.

Measurements and Characterizations: The morphologies of wood were characterized by a SEM (Hitachi SU-70). The transmittance spectrum and haze were measured with a UV–vis Spectrometer Lambda 35 (PerkInElmer, USA). A 532 nm single mode laser DJ532-10 (Thorlabs Inc.) was used as the incoming light source for observing the anisotropic light scattering by the anisotropic film. XRD were collected using multilayered films on a Rigaku RAPID II equipped with a curved detector manufactured by Rigaku Americas Corp (operating tube voltage at 40 kV, tube current at 30 mA, CuKα, $\lambda = 0.1541$ nm). The performance of the transistor was measured by Keithley 2400. A fixed gate voltage and a fixed source–drain voltage were applied, and source–drain current was measured continuously before and after adding the electrolyte. The mechanic properties were performed using a Tinius Olsen H5KT testing machine.

Supporting Information

Supporting Information is available from the Wiley Online Library or from the author.

Acknowledgements

The authors thank Dr. Robert J. Bonenberger in Materials Science & Engineering Department of UMD for the mechanics testing. The authors thank Alfredo J. Diaz and Santiago D. Solares in George Washington University for the AFM characterization. L.H. acknowledges financial support by Air Force of Scientific Research (AFOSR) Young Investigator Program.

Received: November 20, 2016
Revised: January 15, 2017
Published online: March 29, 2017

[1] S. Garner, S. Glaesemann, X. Li, *Appl. Phys. A: Mater. Sci. Process.* **2014**, *116*, 403.
[2] H. Tang, N. Butchosa, Q. Zhou, *Adv. Mater.* **2015**, *27*, 2070.

[3] L. Chen, Q. Wang, K. Hirth, C. Baez, U. P. Agarwal, J. Y. Zhu, *Cellulose* **2015**, *22*, 1753.
[4] Q. Wang, J. Y. Zhu, J. M. Considine, *ACS Appl. Mater. Interfaces* **2013**, *5*, 2527.
[5] Y. H. Jung, T.-H. Chang, H. Zhang, C. Yao, Q. Zheng, V. W. Yang, H. Mi, M. Kim, S. J. Cho, D.-W. Park, H. Jiang, J. Lee, Y. Qiu, W. Zhou, Z. Cai, S. Gong, Z. Ma, *Nat. Commun.* **2015**, *6*, 7170.
[6] M. S. Toivonen, A. Kaskela, O. J. Rojas, E. I. Kauppinen, O. Ikkala, *Adv. Funct. Mater.* **2015**, *25*, 6618.
[7] R. J. Moon, A. Martini, J. Nairn, J. Simonsen, J. Youngblood, *Chem. Soc. Rev.* **2011**, *40*, 3941.
[8] H. Fukuzumi, T. Saito, T. Iwata, Y. Kumamoto, A. Isogai, *Biomacromolecules* **2009**, *10*, 162.
[9] L. Hu, Y. Cui, *Energy Environ. Sci.* **2012**, *5*, 6423.
[10] M. Nogi, S. Iwamoto, A. N. Nakagaito, H. Yano, *Adv. Mater.* **2009**, *21*, 1595.
[11] L. Hu, G. Zheng, J. Yao, N. Liu, B. Weil, M. Eskilsson, E. Karabulut, Z. Ruan, S. Fan, J. T. Bloking, M. D. McGehee, L. Wågberg, Y. Cui, *Energy Environ. Sci.* **2013**, *6*, 513.
[12] A. W. Martinez, S. T. Phillips, G. M. Whitesides, E. Carrilho, *Anal. Chem.* **2010**, *82*, 3.
[13] A. W. Martinez, S. T. Phillips, G. M. Whitesides, *Proc. Natl. Acad. Sci. USA* **2008**, *105*, 19606.
[14] E. Carrilho, A. W. Martinez, G. M. Whitesides, *Anal. Chem.* **2009**, *81*, 1.
[15] Y. H. Lin, H. Ren, S. Gauza, Y. H. Wu, Y. Zhao, J. Fang, S. T. Wu, *J. Disp. Technol.* **2006**, *2*, 21.
[16] A. P. Russell, L. G. Richard, *Formation and Structure of Wood*, American Chemical Society, Washington, DC, USA **1984**.
[17] L. Donaldson, *Wood Sci. Technol.* **2007**, *41*, 443.
[18] J. R. Barnett, V. A. Bonham, *Biol. Rev. Cambridge Philos. Soc.* **2004**, *79*, 461.
[19] P. Xu, L. A. Donaldson, Z. R. Gergely, L. A. Staehelin, *Wood Sci. Technol.* **2007**, *41*, 101.
[20] S. J. Eichhorn, C. A. Baillie, N. Zafeiropoulos, L. Y. Mwaikambo, M. P. Ansell, A. Dufresne, K. M. Entwistle, P. J. Herrera-Franco, G. C. Escamilla, L. Groom, M. Hughes, C. Hill, T. G. Rials, P. M. Wild, *J. Mater. Sci.* **2001**, *36*, 2107.
[21] I. Siró, D. Plackett, M. Hedenqvist, M. Ankerfors, T. Lindström, *J. Appl. Phys.* **2011**, *119*, 2652.
[22] N. Horiuchi, *Nat. Photonics* **2014**, *8*, 172.
[23] L. Nyholm, G. Nyström, A. Mihranyan, M. Strømme, *Adv. Mater.* **2011**, *23*, 3751.
[24] S. J. Eichhorn, A. Dufresne, M. Aranguren, N. E. Marcovich, J. R. Capadona, S. J. Rowan, C. Weder, W. Thielemans, M. Roman, S. Renneckar, W. Gindl, S. Veigel, J. Keckes, H. Yano, K. Abe, M. Nogi, A. N. Nakagaito, A. Mangalam, J. Simonsen, A. S. Benight, A. Bismarck, L. A. Berglund, T. Peijs, *J. Mater. Sci.* **2010**, *45*, 1.
[25] H. Sehaqui, Q. Zhou, O. Ikkala, L. A. Berglund, *Biomacromolecules* **2011**, *12*, 3638.
[26] H. Zhu, S. Zhu, Z. Jia, S. Parvinian, Y. Li, O. Vaaland, L. Hu, T. Li, *Proc. Natl. Acad. Sci. USA* **2015**, *112*, 1.
[27] T. Saito, S. Kimura, Y. Nishiyama, A. Isogai, *Biomacromolecules* **2007**, *8*, 2485.
[28] H. P. S. Abdul Khalil, Y. Davoudpour, M. N. Islam, A. Mustapha, K. Sudesh, R. Dungani, M. Jawaid, *Carbohydr. Polym.* **2014**, *99*, 649.
[29] S. M. Keshk, *J. Bioprocess. Biotech.* **2014**, *4*, 1.
[30] F. Ansari, A. Sjöstedt, P. T. Larsson, L. A. Berglund, L. Wågberg, *Composites, Part A* **2015**, *74*, 60.
[31] A. Rafsanjani, M. Stiefel, K. Jefimovs, R. Mokso, D. Derome, J. Carmeliet, *J. R. Soc., Interface* **2014**, *11*, 20140126.
[32] W. Chen, H. Yu, Y. Liu, P. Chen, M. Zhang, Y. Hai, *Carbohydr. Polym.* **2011**, *83*, 1804.
[33] K. M. O. Håkansson, A. B. Fall, F. Lundell, S. Yu, C. Krywka, S. V Roth, G. Santoro, M. Kvick, L. P. Wittberg, L. Wågberg, L. D. Söderberg, *Nat. Commun.* **2014**, *5*, 4018.
[34] A. K. Yetisen, M. S. Akram, C. R. Lowe, *Lab Chip* **2013**, *13*, 2210.
[35] X. Li, D. R. Ballerini, W. Shen, *Biomicrofluidics* **2012**, *6*, 12.
[36] J. Jin, J. Lee, S. Jeong, S. Yang, J.-H. Ko, H.-G. Im, S.-W. Baek, J.-Y. Lee, B.-S. Bae, *Energy Environ. Sci.* **2013**, *6*, 1811.
[37] H. Zhu, Z. Fang, C. Preston, Y. Li, L. Hu, *Energy Environ. Sci.* **2014**, *7*, 269.
[38] T. R. Mattsson, J. M. D. Lane, K. R. Cochrane, M. P. Desjarlais, A. P. Thompson, F. Pierce, G. S. Grest, *Phys. Rev. B: Condens. Matter Mater. Phys.* **2010**, *81*, 54103.
[39] S. Plimpton, *J. Comput. Phys.* **1995**, *117*, 1.
[40] D. H. Tsai, *J. Chem. Phys.* **1979**, *70*, 1375.
[41] J. A. Zimmerman, E. B. Webb III, J. J. Hoyt, R. E. Jones, P. A. Klein, D. J. Bammann, *Comput. Fluid Solid Mech.* **2003**, *319*, 804.

ADVANCED MATERIALS

Supporting Information

for *Adv. Mater.*, DOI: 10.1002/adma.201606284

Anisotropic, Transparent Films with Aligned Cellulose Nanofibers

*Mingwei Zhu, Yilin Wang, Shuze Zhu, Lisha Xu, Chao Jia, Jiaqi Dai, Jianwei Song, Yonggang Yao, Yanbin Wang, Yongfeng Li, Doug Henderson, Wei Luo, Heng Li, Marilyn L. Minus, Teng Li, and Liangbing Hu**

Supporting Information

Anisotropic, Transparent Films with Aligned Cellulose Nanofibers

Mingwei Zhu,[1] Yilin Wang,[1] Shuze Zhu,[2] Lisha Xu,[1] Chao Jia,[1] Jianwei Song,[1] Yonggang Yao,[1] Yanbin Wang,[1] Yongfeng Li,[1] Doug Henderson,[1] Wei Luo,[1] Heng Li[3], Marilyn L. Minus,[3] Teng Li,[2] Liangbing Hu[1,*]

[1]Department of Materials Science and Engineering, University of Maryland, College Park, Maryland, 20742, USA
[2]Department of Mechanical Engineering, University of Maryland, College Park, Maryland, 20742, USA
[3]Department of Mechanical and Industrial Engineering, Northeastern University, Boston, Massachusetts, 02115, USA

Email: binghu@umd.edu

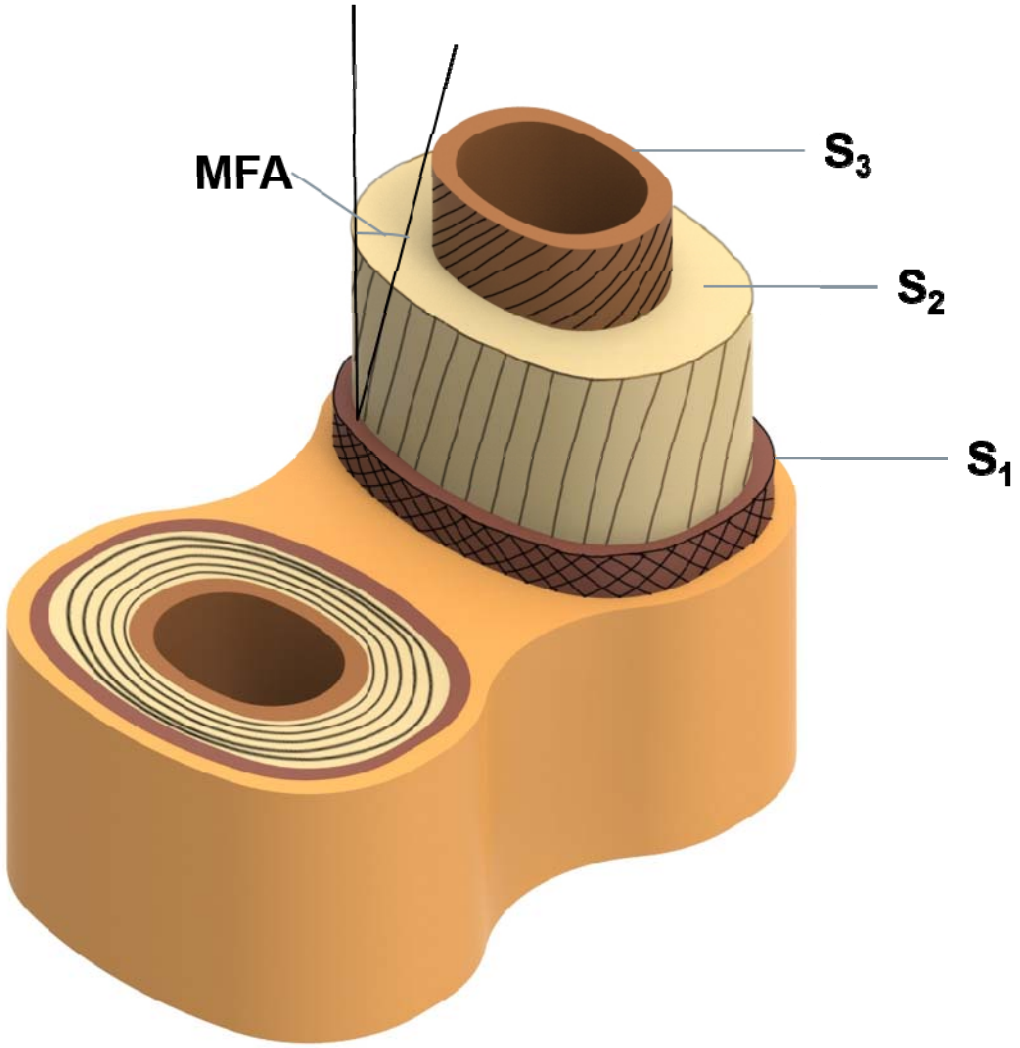

Figure S1. Typical wood cell wall microstructures. The cell wall of wood is typically composed of the primary wall (P) and the secondary wall (S). The second layer consists of three layers (S1, S2 and S3). Among them, the aligned S2 layer makes up the vast majority of the cell wall. (Figure Modified from J. R. Soc. Interface 11: 20140126, 2014)

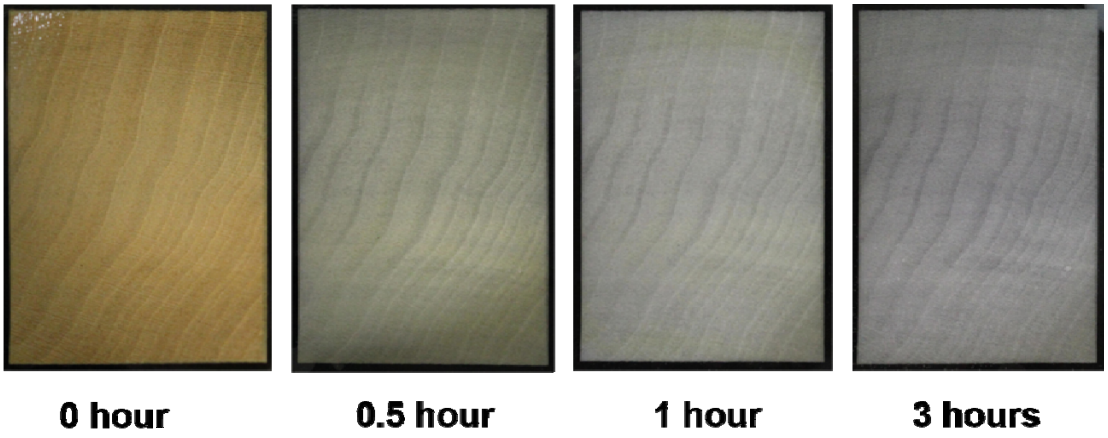

Figure S2. Delignification process using NaClO as the lignin removal chemical. The wood color changes from yellow to white gradually with increasing delignification time (45° cutting direction).

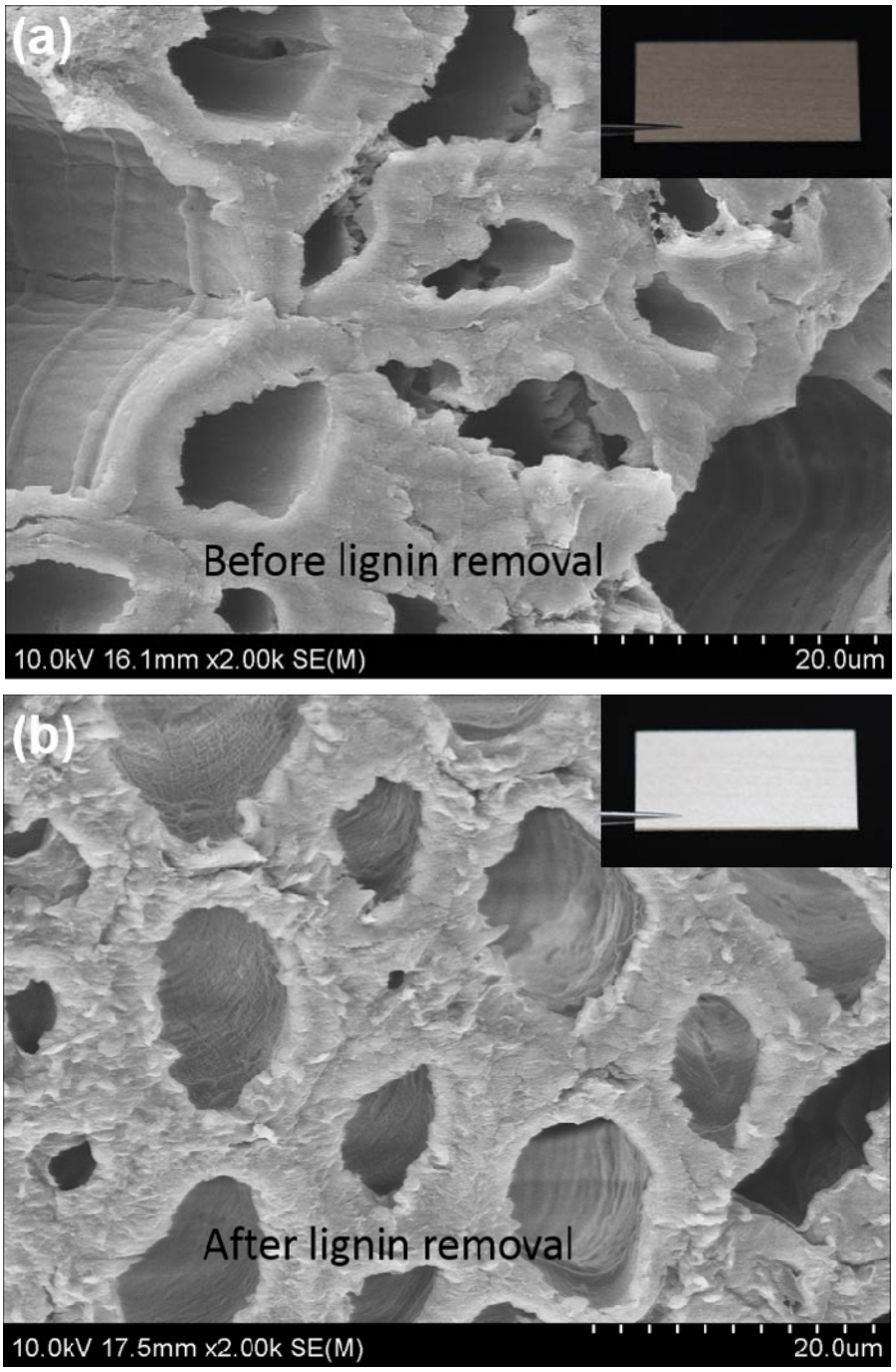

Figure S3. SEM images of wood before (a) and after lignin removal (b). The structure of wood is well preserved after delignification.

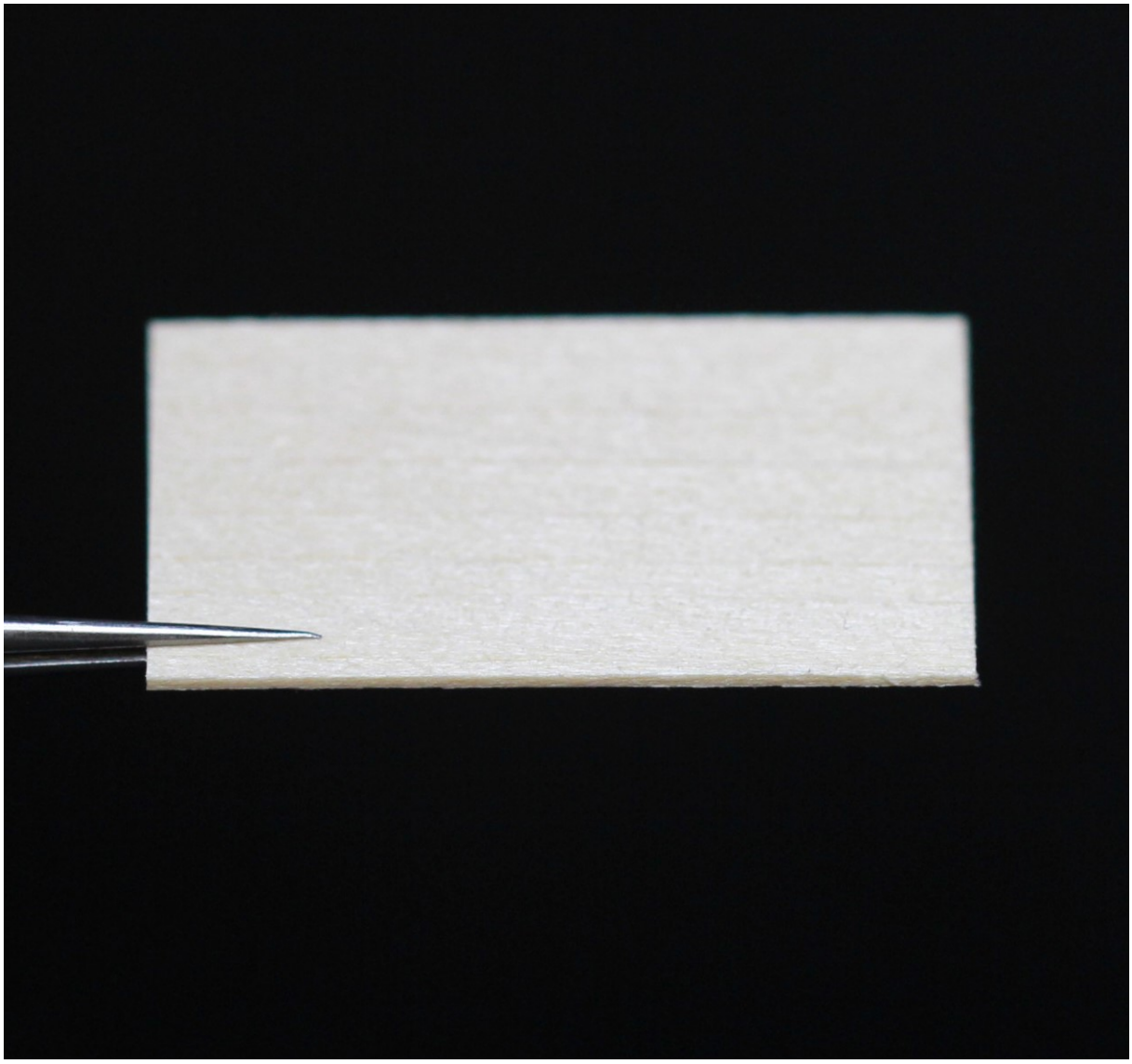

Figure S4. Photo of the lignin removed wood sample. After lignin removal, wood becomes white and its microstructures can be well preserved.

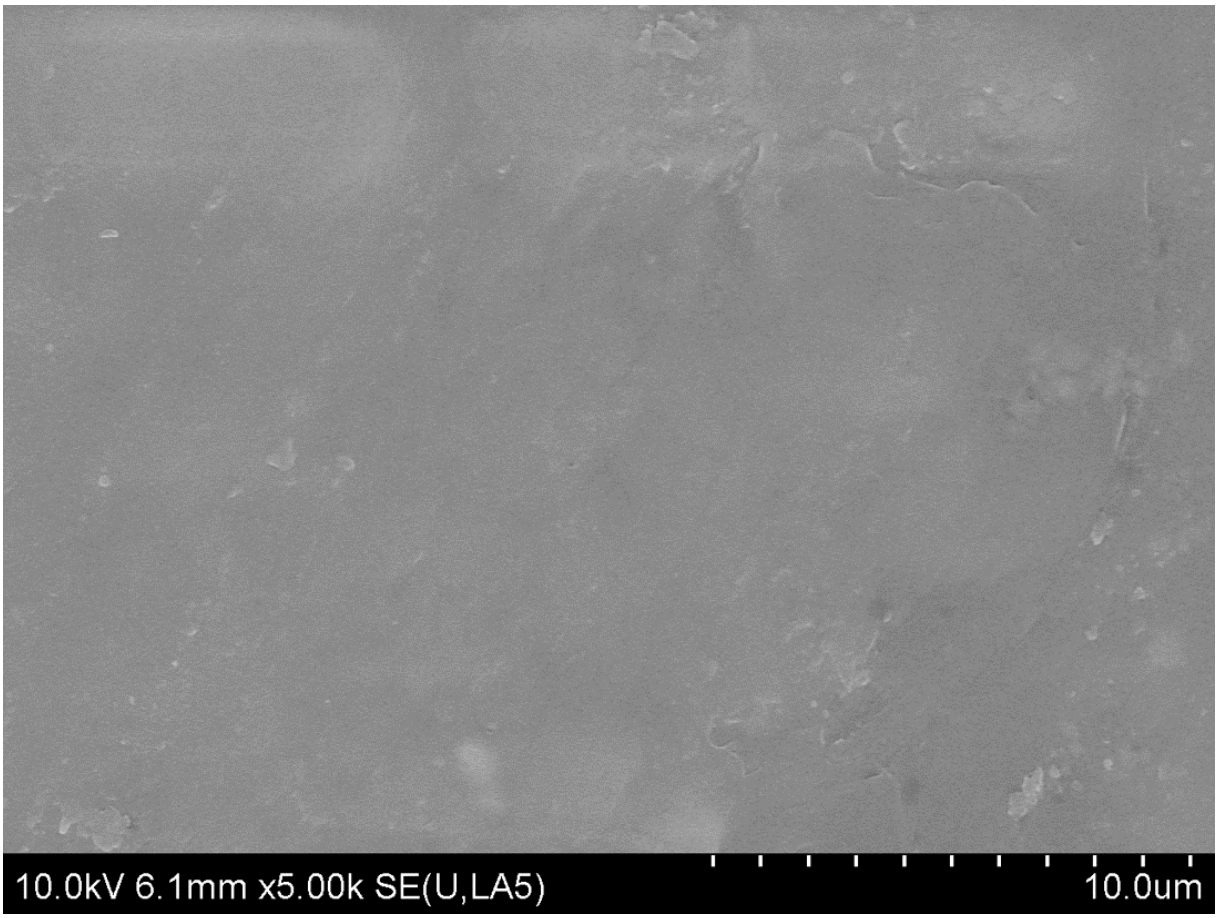

Figure S5. SEM image of the surface of a transparent anisotropic film. The film surface is flat.

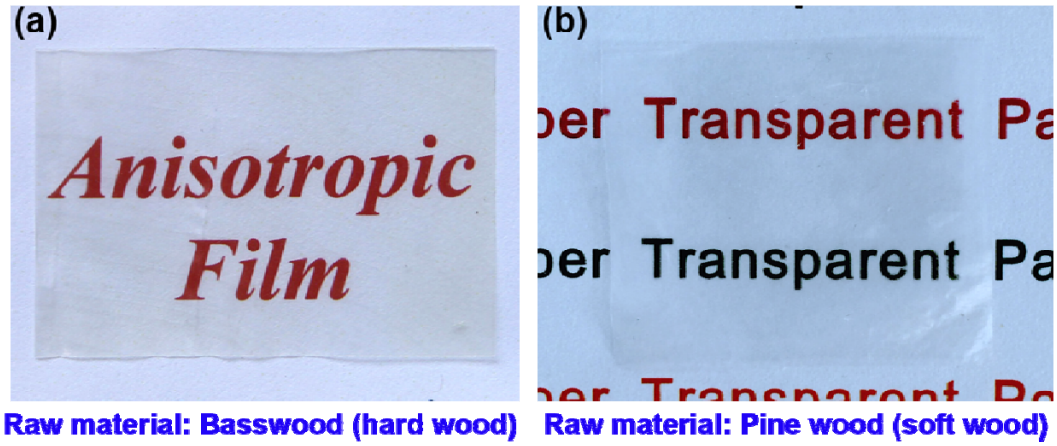

Figure S6. Transparent, anisotropic films fabricated from basswood (a) and pine wood (b).

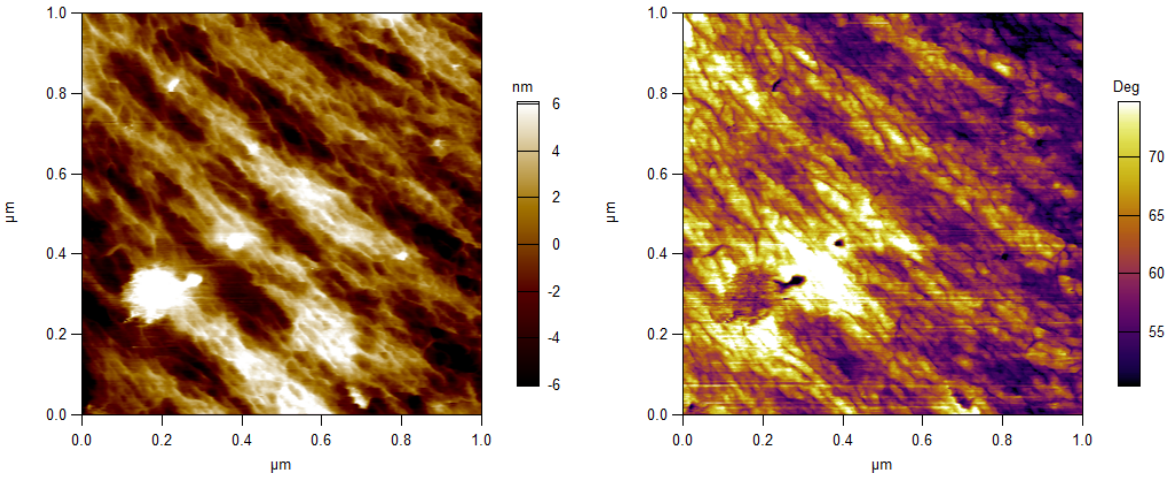

Figure S7. AFM images (height and phase images) of the anisotropic transparent film.

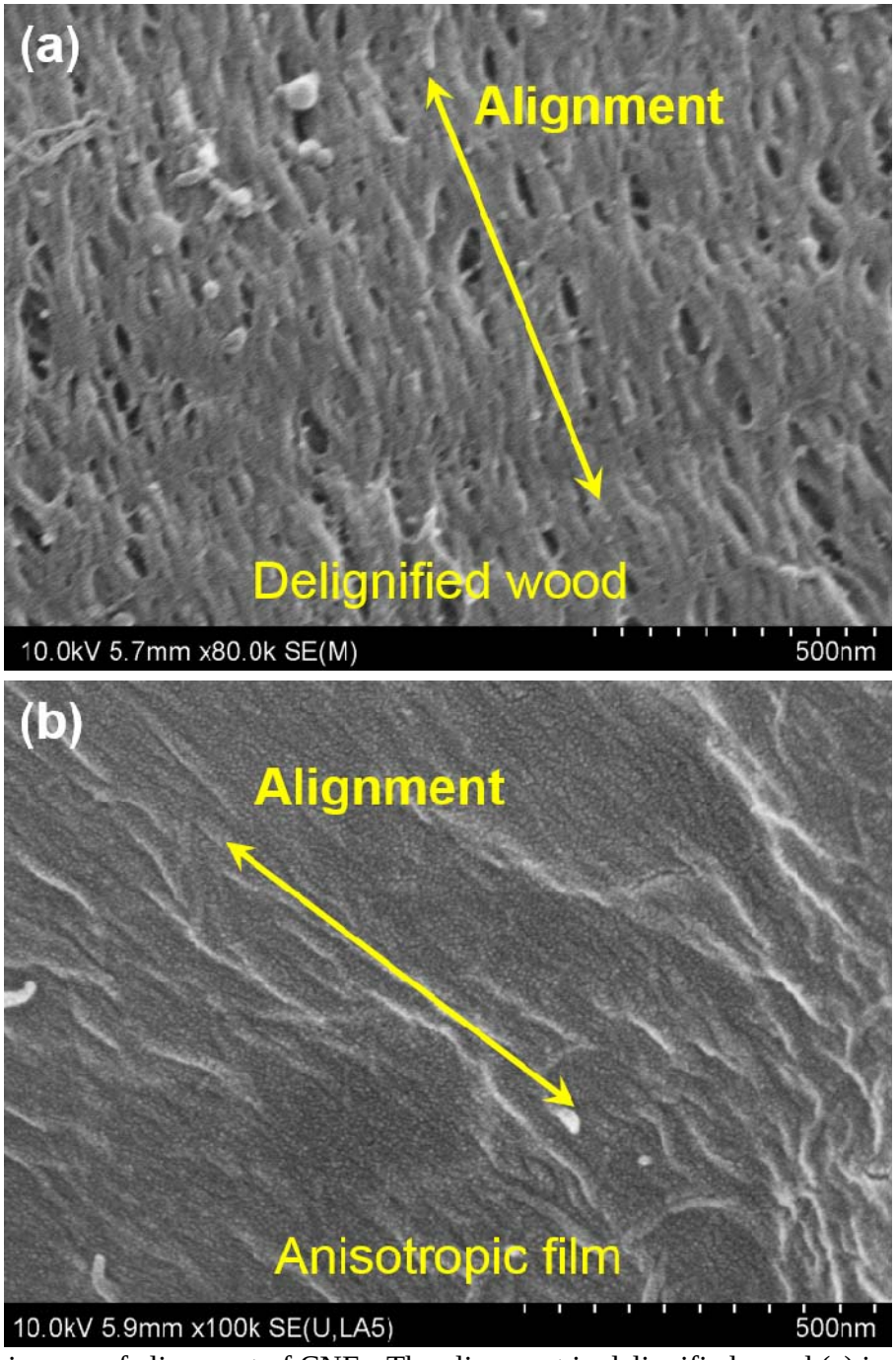

Figure S8. SEM images of alignment of CNFs. The alignment in delignified wood (a) is well preserved after pressing (b).

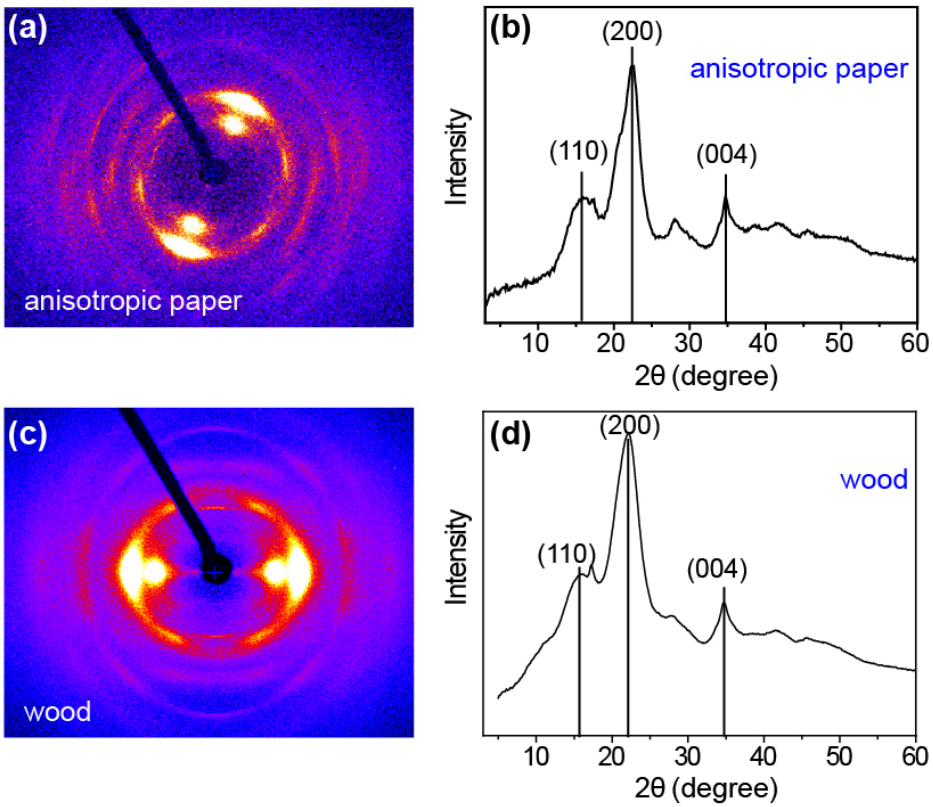

Figure S9. XRD analysis of transparent film (a and b) and wood (c and d). The lignification and pressing fabrication processes do not change the CNF alignment.

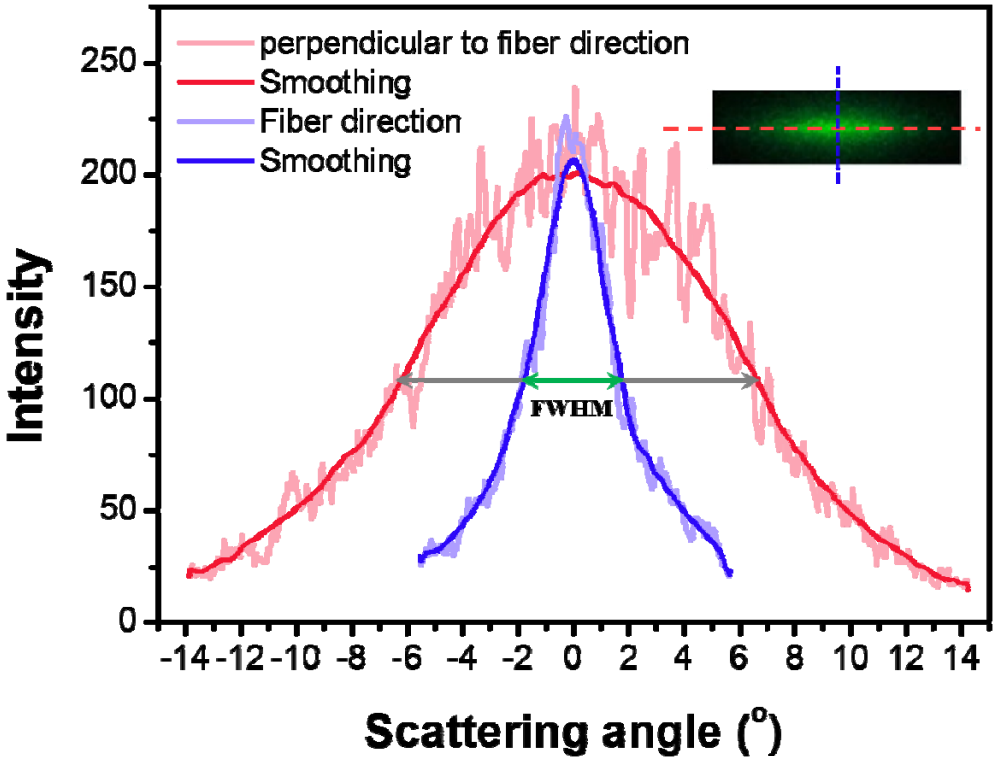

Figure S10. The light intensity distributions in the film along and perpendicular to the fiber directions. The optical transmittance of the film shows strong anisotropic behavior. The full width at half maximum (FWHM) perpendicular to the fiber direction is about 3.5 times of the value along the fiber direction.

We used a polarizing microscope with two linear polarizers, which can be oriented in the horizontal and vertical position, respectively. The anisotropic film is placed between the two polarizers with the direction of fiber alignment parallel to the direction of the first polarizer, where the position is set as 0º. Then the two polarizers are fixed and the film is rotated counter-clockwise with 90º interval. A CCD camera is used to capture the light transmitted from the second polarizer for imaging. The experimental results are shown in Figure S11.

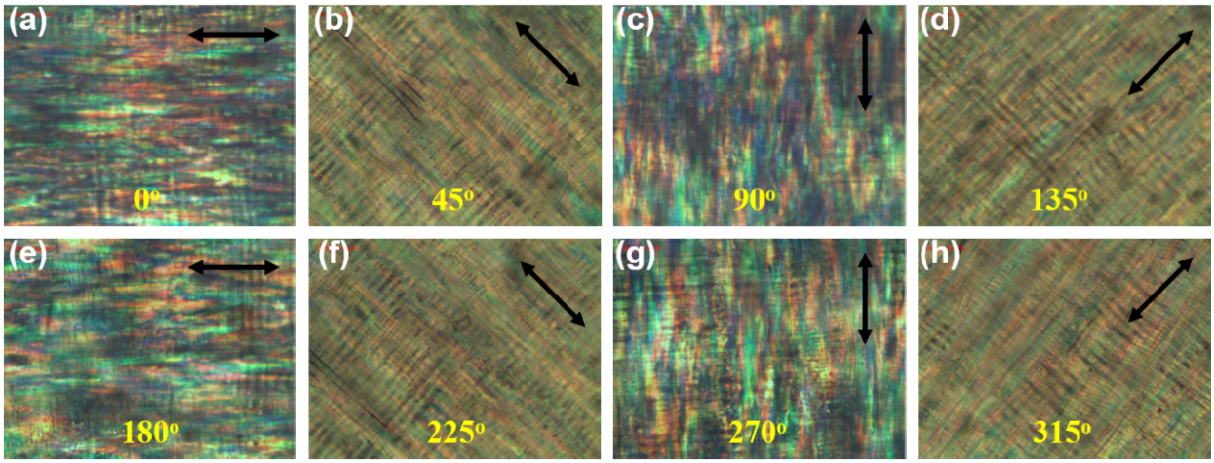

Figure S11. The polarization effect of the anisotropic film observed by a cross-polarized microscope. The black arrows indicate the fiber alignment direction in the anisotropic film.

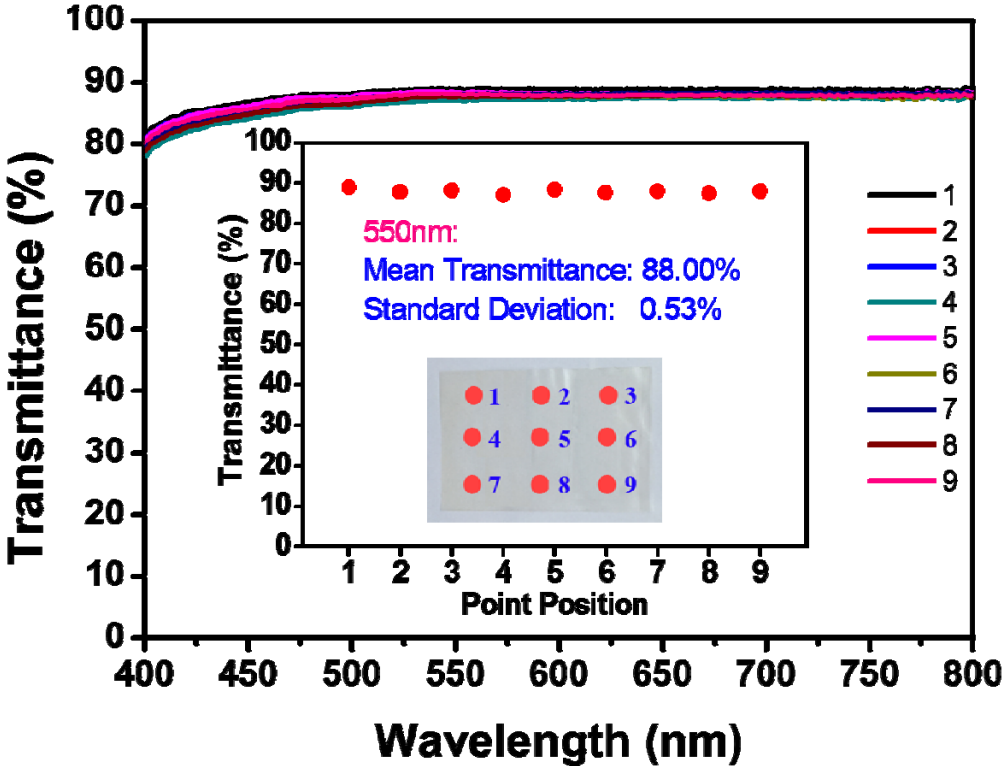

Figure S12. The transmittance of the film measured at different positions.

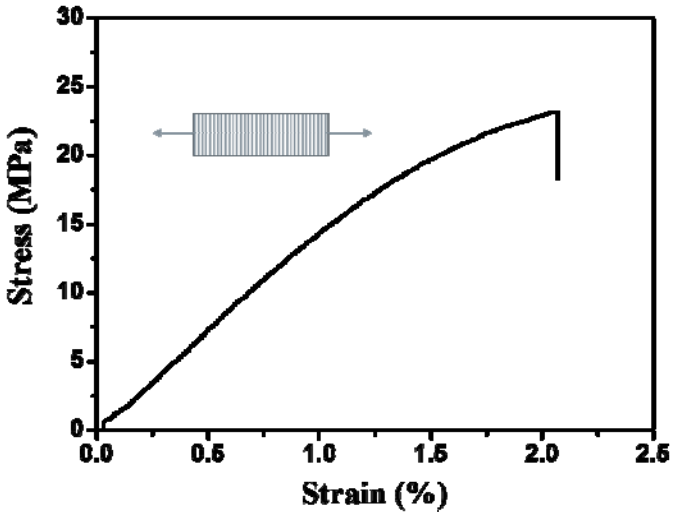

Figure S13. The stress-strain curve along the direction perpendicular to the nanofiber alignment direction.

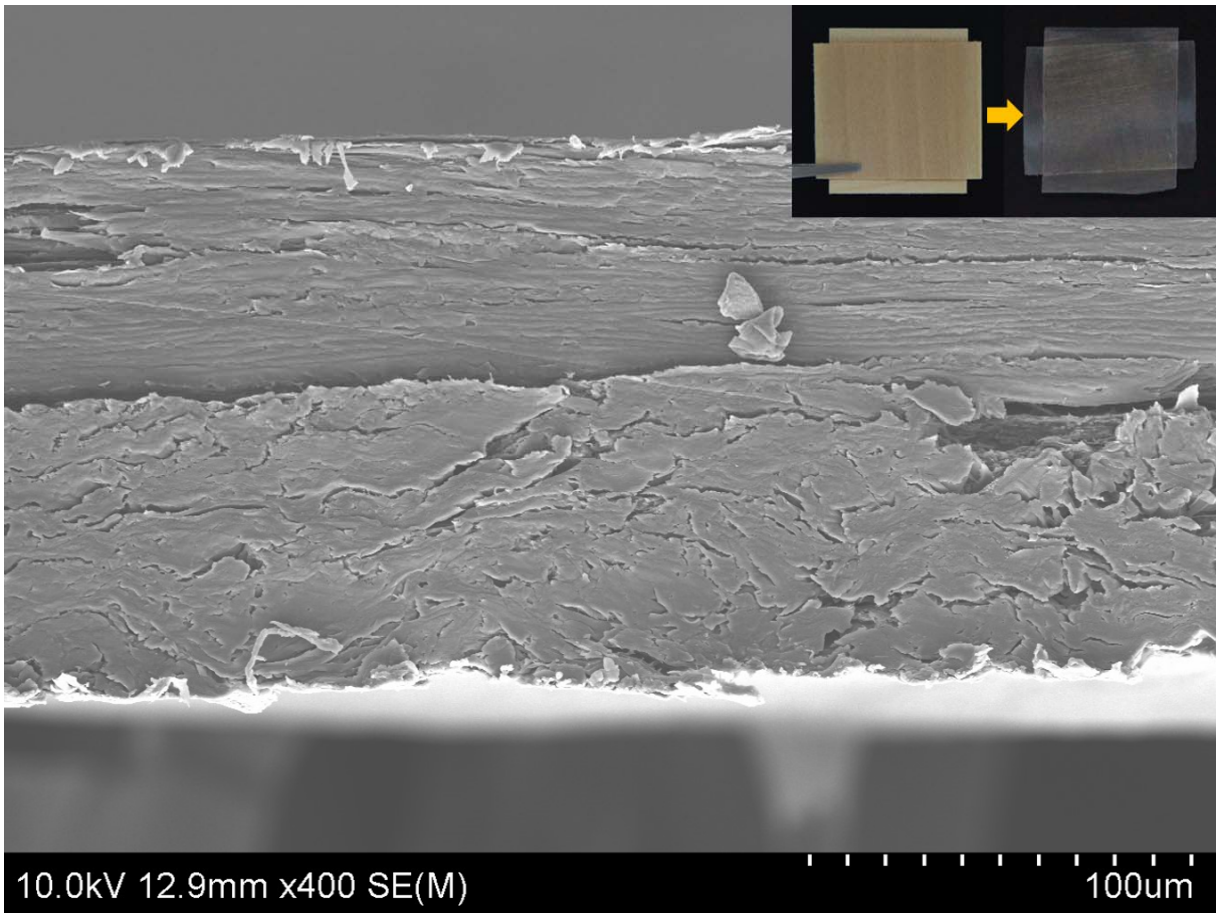

Figure S14. SEM image of a transparent film made of two cross-stacked anisotropic films. The lumina in the upper layer are along the film surface and the lumina in the lower layer are perpendicular to the film surface.

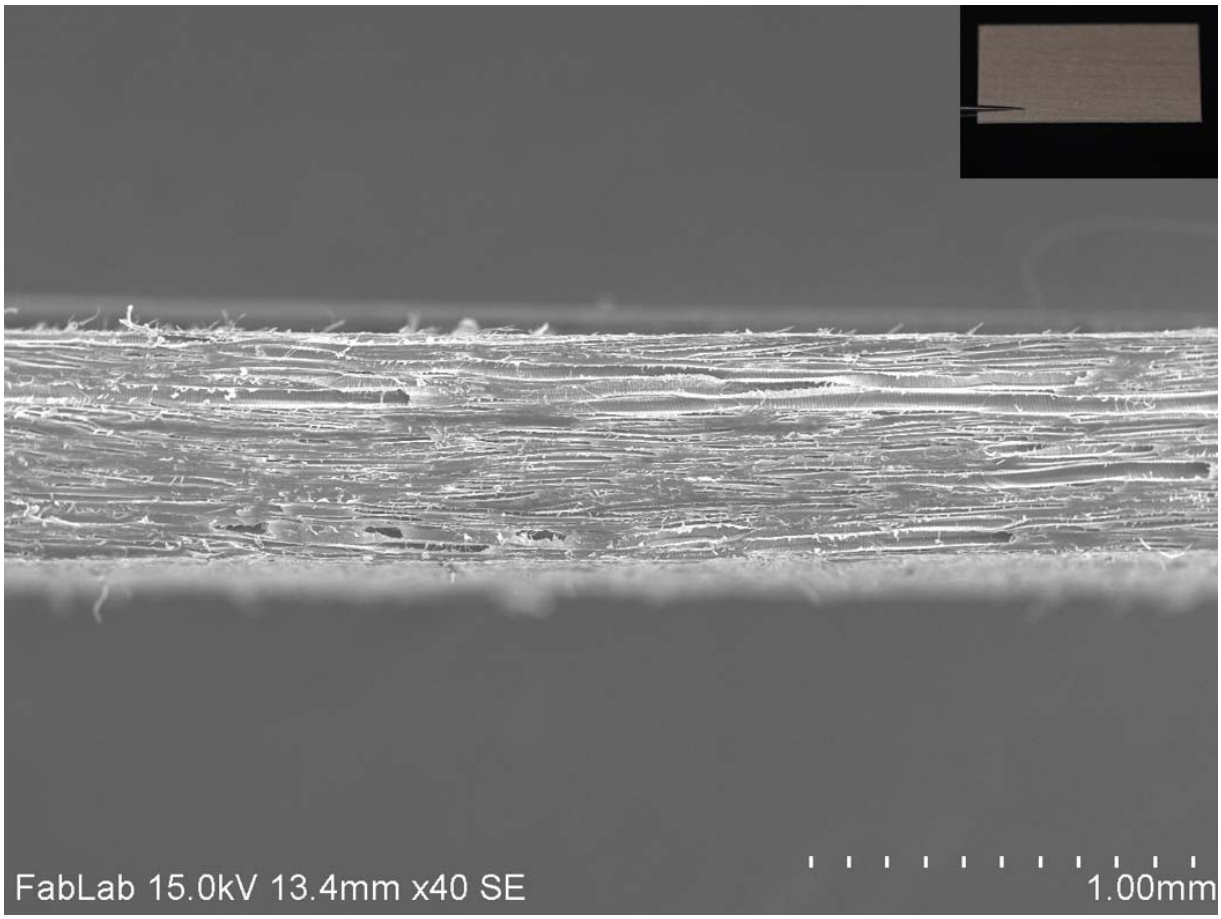

Figure S15. SEM image of a wood slice with 0° cutting direction. The lumina in wood are well aligned along the cutting direction.

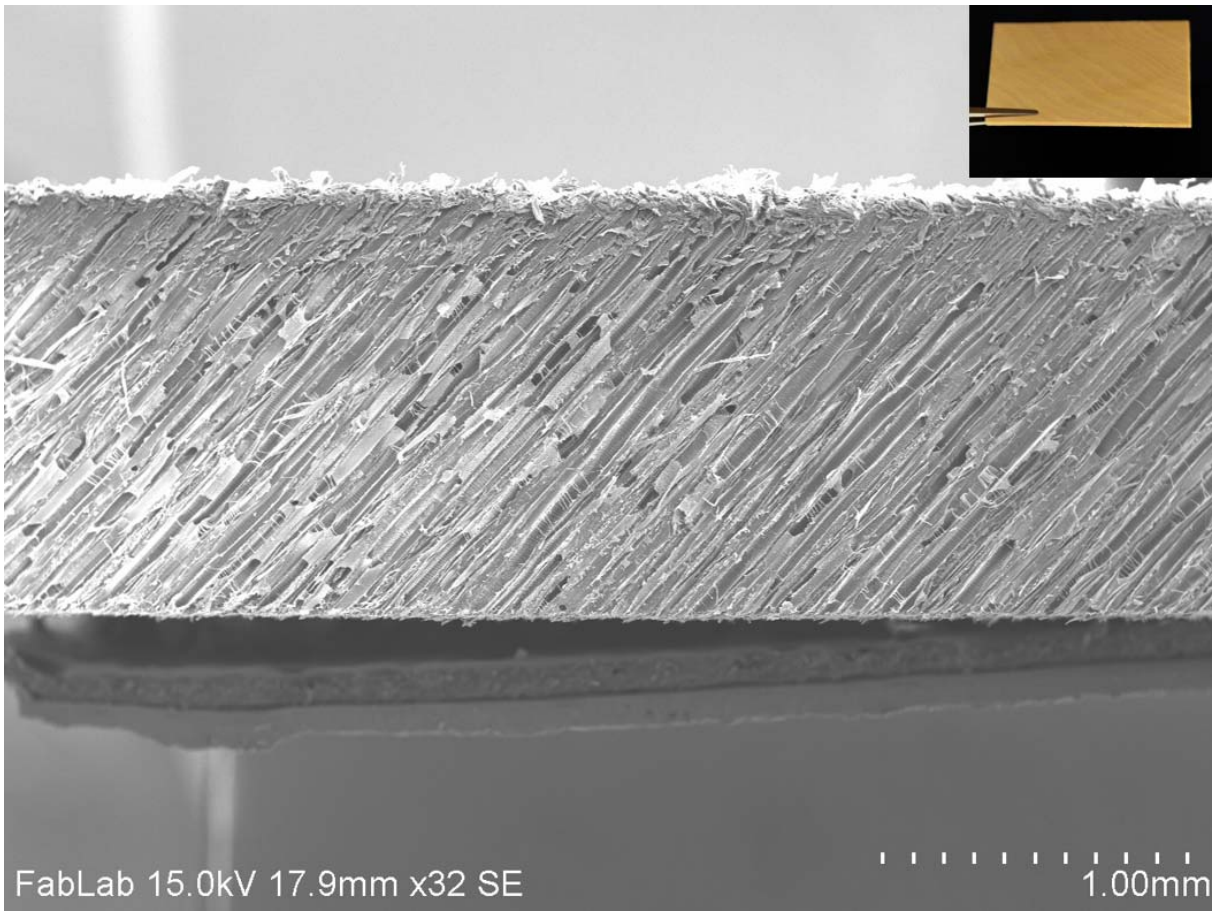

Figure S16. SEM images of a wood slice with 45° cutting direction**.** The lumina in wood are aligned with 45° deviation from the cutting direction.

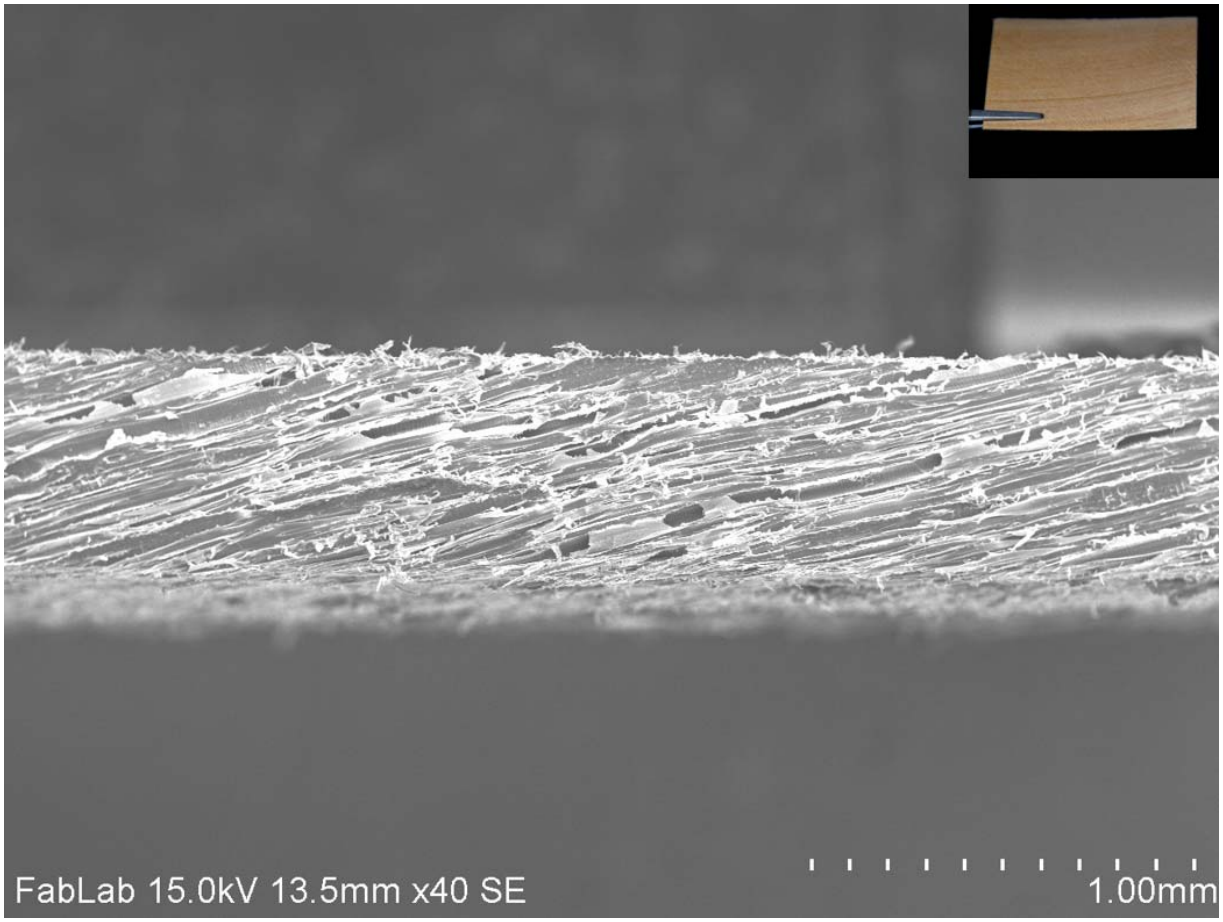

Figure S17. SEM images of a wood slice with 22.5° cutting direction. The lumina in wood are aligned with 22.5° deviation from the cutting direction.

Molecular dynamics simulations

The full atomistic simulations use the ReaxFF potential simulation package [38,39]. The time step is 0.5 fs.

For each cellulose chain, all the oxygen atoms on the backbone of each cellulose chain are treated as a single rigid body. Such a treatment could prevent excessive bending of cellulose chains during loading and therefore we can focus on analyzing the interplay between alignment, interfacial sliding, and hydrogen bonding.

The construction of the well-aligned model is shown in Figure S18 (a). For equilibration, the system is subjected to NPT ensemble at a pressure of 1 atmosphere (normal pressure controlled independently) and at a temperature of 300K, using Nosé-Hoover thermostat. Such a run lasts for 200000 time steps. Figure S18(b) shows the pressure-equilibrated structure. Then the mechanical deformation is applied by uniformly deforming the simulation box parallel to the chain alignment direction (horizontally) or perpendicular to the chain alignment direction (vertically) at a constant engineering strain rate of 0.0000025/fs, while the system is subjected to NVT ensemble with the temperature unchanged.

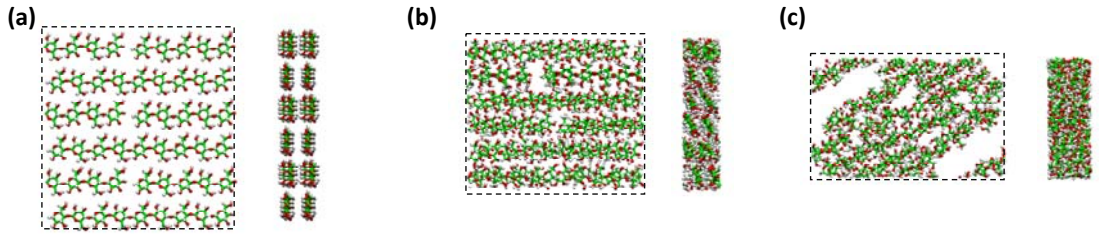

Figure S18. (a) Initial well-aligned model, top view and side view. There are in total 12 cellulose chains (each has nine hexagon rings) in a periodical simulation box (dashed line). Three alternating rows of cellulose chains are horizontally displaced about half the simulation box length. Green: carbon. Gray: hydrogen. Red: Oxygen. (b) Pressure-equilibrated well-aligned model. (c) Pressure-equilibrated tilted model.

Construction of Tilted Model

The construction of the tilted model follows several steps: 1) Construct a very large simulation box and put 12 parallel cellulose chains inside it so that initially they don't feel each other. 2) Impose restrains that these chains can only move along their backbone length direction. 3) Run NVT simulations and gradually shrink the simulation box size so that these cellulose chains start to aggregate. The target simulation box size is set to the one shown in Figure S18 (b). 4) Run NPT simulations to equilibrate. After this step, the mechanical deformation is applied in the same way as previously described.

Figure S19 shows the deformation trajectory snapshots for the three models under consideration. The virial stress is commonly used to relate to the macroscopic (continuum) stress in molecular dynamics computations [40,41]. At every time step during the loading, the virial stress per atom (with the unit of pressure*atomic volume) is computed from LAMMPS. To reduce random and temperature-related stress fluctuations, we average the computed stress data within every 30000 time steps, by summing up the virial stress of every atom in the system and averaged over the occupied volume of all the atoms, which we take as the volume of the simulation box after equilibration. The loading is applied along x direction (horizontal) and we plot the normal virial stress tensor component along x direction against the engineering strain. The engineering strain is defined as the increment of the box size along x direction divided by its initial length.

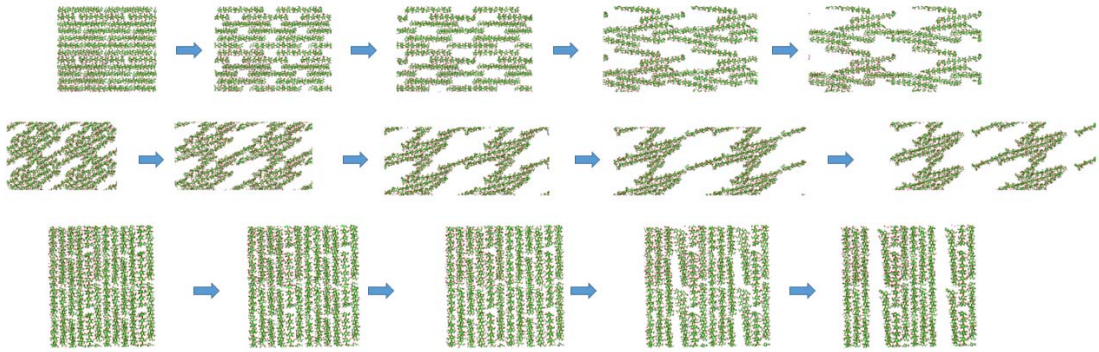

Figure S19. Representative deformation trajectory snapshots for parallel, tilted, and perpendicular models. Here four periodic images are patched together for visual clarification.